Dynamically tunable three-color reflections immune to disorder in optical lattices with trapped cold ^{87}Rb atoms

Hong Yang,[1] Tinggui Zhang,[2] Yan Zhang,[3,*] and Jin-Hui Wu[3,†]

[1]*School of Physics and Electronic Engineering, Hainai Normal University, Haikou 571158, People's Republic of China*

[2]*School of Mathematics and Statistics, Hainai Normal University, Haikou 571158, People's Republic of China,*

[3]*School of Physics, Northeast Normal University, Changchun 130024, People's Republic of China*

(Received 22 December 2019; revised manuscript received 30 April 2020; accepted 5 May 2020; published 26 May 2020)

We investigate a four-level tripod atomic sample trapped, respectively, in a one-dimensional order and disorder (atom number fluctuation) optical lattice to achieve the tunable and robust three-color reflections in the regimes of zero absorption. Based on electromagnetically induced transparency (EIT) and the periodic modulation of the atom number density, there are three reflection regions of high probe reflectivity in different frequency ranges, respectively. Such three-color reflections arise from the double-EIT atomic structure in the optical lattice and can also be observed by the suppression of the density of photonic states. One of them appears in the large detuning range, and the other two locate in two EIT windows, respectively, which are relatively narrow and can be dynamically manipulated flexibly. It is worth noting that such reflection scheme has strong robustness, i.e., it is immune to the atom number fluctuation in the disorder structure. Our results have potential applications in all-optical networks with respect to fabricating efficient devices (such as reflectors and diodes) for manipulating multicolor photon flows.

DOI: 10.1103/PhysRevA.101.053856

I. INTRODUCTION

In the past few decades, artificially optical materials, which have almost arbitrary variations of material properties that are not available in natural mediums, have provided an enormous degree of freedom for the control of light propagation [1–3]. Among them, as a prominent metamaterial, the photonic crystal (PC), famous for its photonic band gaps (PBGs), has been extensively studied [4–7]. In recent years, much effort has been devoted to fabricate PCs in the visible-wavelength range, even in the near-infrared communication band [8–10]. Due to the periodical spatial modulation of the refractive index in a PC, PBGs arise near the Brillouin-zone boundaries [11–15]. For the strong confinement of light, PBGs are widely applied in light storage [16], high-precision sensing [17], ultrafast optical switch [18], integrated photonic circuits [19], low-threshold nanolasers [20], and so on.

However, once the traditional PC is generated, the periodic structure will no longer change, and thus the PBG structure is almost fixed. Typically, additional freedom of light manipulation using PBGs can be provided by the regime of the optical lattice trapping cold atoms of Gaussian density distribution in each period [21,22], which has been used to fabricate non-Hermitian optical materials of parity-time ($\mathcal{PT}$) symmetry or antisymmetry [23–25], and realize dynamically controlled PBGs theoretically and experimentally [26–30]. The other regime for tunable PBGs is the uniformly distributed atomic system driven by coherent standing-wave (SW) fields based on electromagnetically induced transparency (EIT) [31–36]. Under the Bragg scattering condition, PBGs arise from the periodic atomic density distribution in the first regime and the periodic atomic coherences induced by the resonant coupling from the SW field in the other one. Furthermore, such a modulation relies on the order and periodicity of those structures [37–39]. Thus, it is expected that more applications of those regimes will be explored, such as the modulation of multicolor photon flows. However, in the optical lattice, the imperfect manufacturing process or random distributions of atoms may destroy the periodicity, so the disorder should be considered for generating PBGs [24,40–42]. Disorder plays a crucial role in the dynamic control of interacting particles and transport properties of quantum systems [43,44]. Thus, we will realize the multicolor PBGs in the atomic lattices driven by traveling-wave fields and maintain the robustness of light propagation.

In this paper, we propose a scheme for studying photonic properties, respectively, in a one-dimensional (1D) order and disorder optical lattice fulfilled with Gaussian-distribution cold ^{87}Rb atoms driven into a four-level tripod-type EIT configuration by traveling-wave coupling fields. This paper is organized as follows. Section II is devoted to the theoretical description of such a system. e.g., the fixed system of the atomic lattice interacting with proper coupling laser beams and the equations for calculating the probe susceptibility, dispersion relation, and the density of photonic state (DOS). Section III exhibits the three reflection regions appearing in two EIT windows and in an off-resonant range, respectively. Results show that two PBGs in the regime of EIT are more

*zhangy345@nenu.edu.cn

†jhwu@nenu.edu.cn

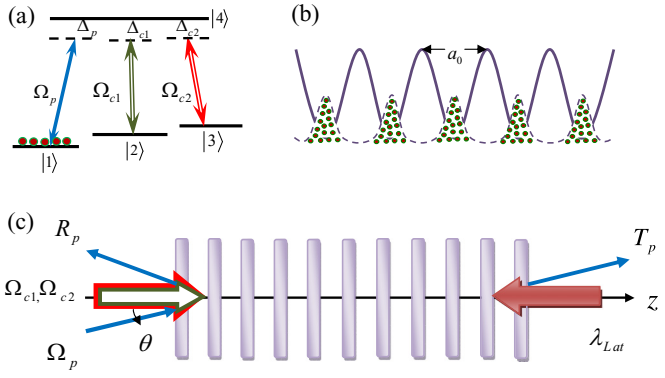

FIG. 1. (a) Energy-level diagram form of a four-level tripod-type atomic system interacting with a weak probe field of Rabi frequency (detuning) Ω_p (Δ_p) and two strong-coupling fields of Rabi frequencies (detunings) Ω_{c1} (Δ_{c1}) and Ω_{c2} (Δ_{c2}), respectively. (b) Scheme of one-dimensional optical lattice of periodicity a_0 filled with these driven tripod atoms. (c) Probe and coupling fields travel along the lattice axis z, and the probe field has a small angle θ relative to the z axis.

sensitive to the frequency and intensity of coupling fields, the width of the atomic distribution, and geometric Bragg detuning of the optical lattices. Note that the photonic properties have very strong robustness, i.e., immune to a common kind of disorder (the atom number fluctuation) in the optical lattice. Section IV gives a conclusion.

II. MODEL AND METHODS

Our atomic configuration is shown in Fig. 1(a). Here we consider that an ensemble of cold ^{87}Rb atoms are driven into a four-level tripod system, where a weak field of frequency ω_p (amplitude $\mathbf{E}_p$) probes transition $|1\rangle \leftrightarrow |4\rangle$ of wavelength λ_{41}, a coupling field of the frequency ω_{c1} (amplitude $\mathbf{E}_{c1}$) drives transition $|2\rangle \leftrightarrow |4\rangle$, and the other frequency ω_{c2} (amplitude $\mathbf{E}_{c2}$) drives $|3\rangle \leftrightarrow |4\rangle$. The corresponding Rabi frequencies (detunings) are $\Omega_p = \mathbf{E}_p \cdot \mathbf{d}_{14}/2\hbar$ ($\Delta_p = \omega_{41} - \omega_p$), $\Omega_{c1} = \mathbf{E}_{c1} \cdot \mathbf{d}_{24}/2\hbar$ ($\Delta_{c1} = \omega_{42} - \omega_{c1}$), and $\Omega_{c2} = \mathbf{E}_{c2} \cdot \mathbf{d}_{34}/2\hbar$ ($\Delta_{c2} = \omega_{43} - \omega_{c2}$), with $\mathbf{d}_{ij}$ and ω_{ij} being dipole moments and resonant frequencies on relevant transitions. To be more concrete, levels $|1\rangle$, $|2\rangle$, $|3\rangle$, and $|4\rangle$ may refer to $|5S_{1/2}, F = 1, m_F = 0\rangle$, $|5S_{1/2}, F = 1, m_F = -1\rangle$, $|5S_{1/2}, F = 1, m_F = 1\rangle$, and $|5P_{3/2}, F = 1, m_F = 0\rangle$ of ^{87}Rb atoms' D2 line broken by static magnetic fields in order. Such a tripod structure can also correspond to hyperfine levels of ^{87}Rb atoms with the D1 line [45]. These atoms are trapped in a 1D optical lattice of the periodicity a_0 with Gaussian density distribution within each lattice as shown in Fig. 1(b). The optical lattice is formed by a red-detuned retroreflected laser beam of wavelength $\lambda_{\rm Lat} = 2a_0$ along the z-axis lattice direction. In Fig. 1(c), two coupling fields transmit along the z axis, while the probe field has a little angle θ ($\cos\theta = \lambda_p/\lambda_{\rm Lat}$) relative to z. To our attention, the relation $\lambda_{\rm Lat} > \lambda_{41}$ should be satisfied in order to trap atoms.

In each period, the atom number density along z is

$$N_k(z) = \frac{N_0(1 + \Delta j_{\rm Rand})a_0}{\sigma_z\sqrt{2\pi}} e^{\left[-(z-z_k)^2/2\sigma_z^2\right]}, \tag{1}$$

with the average atomic density N_0, the kth lattice center $z_k = (k - 1/2)a_0$ with periodicity $a_0 = \Delta\lambda_{\rm Lat}/2$, and the half width $\sigma_z = \lambda_{\rm Lat}/(2\pi\sqrt{\eta})$ where $\eta = 2U_0/(\kappa_B T)$ is related to the trapping depth U_0 of the optical potential and the temperature T of the atomic sample. In particular, it seems that the width $\sigma_z \to 0$ when $T \to 0$; however, when $T \to 0$ and $\sigma_z \ll a_0$, the width σ_z should be limited by the size of the Wannier function in a given lattice minimum, which could be approximated by the ground state of the harmonic approximation close to the minima. In addition, $\Delta j_{\rm Rand}$ ($|\Delta j_{\rm Rand}| \leqslant 1$) varying along z are the random numbers corresponding to the atom number fluctuation so that $N_0(1 + \Delta j_{\rm Rand})$ can describe a kind of disorder, i.e., the atom number fluctuation in this 1D lattice. Here, we set density N_0 to be relatively small, i.e., 7×10^{11} cm^3 hereafter, so that the average distance between two atoms is much longer than the size of each atom. Thus, the interaction of atoms can be neglected here, when the temperature T ($\sim$140 μK) is not ultralow. In addition, the alkaline-earth atoms such as Yb may also be trapped in an optical lattice and then be used in such a study [46,47].

Under the rotating-wave and electric-dipole approximations, the atom-field interaction Hamiltonian is

$$\begin{aligned} H_I = {} & \hbar[(\Delta_p - \Delta_{c1})|2\rangle\langle 2| + (\Delta_p - \Delta_{c2})|3\rangle\langle 3| + \Delta_p|4\rangle\langle 4|] \\ & - \hbar[\Omega_p|4\rangle\langle 1| + \Omega_{c1}|4\rangle\langle 2| + \Omega_{c2}|4\rangle\langle 3| + \text{H.c.}]. \end{aligned} \tag{2}$$

Then, the equations of motion of the density matrix are written as

$$\begin{aligned} \partial_t\rho_{21} &= [i(\Delta_{c1} - \Delta_p) - \gamma_{21}]\rho_{21} - i\Omega_p\rho_{24} + i\Omega_{c1}^*\rho_{41}, \\ \partial_t\rho_{31} &= [i(\Delta_{c2} - \Delta_p) - \gamma_{31}]\rho_{31} - i\Omega_p\rho_{34} + i\Omega_{c2}^*\rho_{41}, \\ \partial_t\rho_{41} &= -(i\Delta_p + \gamma_{41})\rho_{41} + i\Omega_p(\rho_{11} - \rho_{44}) \\ &\quad + i\Omega_{c1}\rho_{21} + i\Omega_{c2}\rho_{31}, \end{aligned} \tag{3}$$

with the conjugation condition $\rho_{ij} = \rho_{ji}^*$. Here, $\gamma_{ij} = (\Gamma_i + \Gamma_j)/2$ denotes the complex coherence dephasing rate with $\Gamma_i = \sum_m \Gamma_{im}$, $\Gamma_j = \sum_n \Gamma_{jn}$ being population decay rates. In the weak probe limit of $\Omega_p \ll \Omega_{c1,c2}$, constrained by $\rho_{11} \simeq 1$, $\rho_{22} \simeq \rho_{33} \simeq \rho_{44} \simeq 0$. Density matrix equations can be solved in the steady state $\partial t\rho_{ij} = 0$,

$$\rho_{41} = \frac{\Omega_p^*}{\frac{|\Omega_{c1}|^2}{\Delta_p - \Delta_{c1} - \gamma_{21}} + \frac{|\Omega_{c2}|^2}{\Delta_p - \Delta_{c2} - \gamma_{31}} + \gamma_{41} - \Delta_p}. \tag{4}$$

The complex probe susceptibility in this atomic medium yields

$$\chi_p(z) = \chi_p'(z) + i\chi_p''(z) = \frac{N_k(z)|d_{41}|^2}{\varepsilon_0\hbar}\frac{\rho_{41}}{\Omega_p}, \tag{5}$$

and the spatially periodic refractive index $n_p(z) = \sqrt{1 + \chi_p(z)}$, depending on the modulation of the atom polarizability. Here we further rewrite $\cos\theta = \lambda_{p0}/\lambda_{\rm Lat0}$ in the vacuum with $\lambda_{p0}/\lambda_p = \lambda_{\rm Lat0}/\lambda_{\rm Lat} = n_p$, which means that the "geometric" Bragg condition with the shift $\Delta\lambda_{\rm Lat} = \lambda_{\rm Lat} - \lambda_{\rm Lat0}$ requires nonzero propagation angle θ. Subject to this condition,

$$\chi_p' + i\chi_p'' \simeq \frac{-2\Delta\lambda_{\rm Lat}}{\lambda_{\rm Lat}}, \tag{6}$$

which can predict the point of Δ_p for reflective bands appearing [28,30].

The reflection and transmission properties can be described by a 2×2 unimodular transfer matrix m_p of each lattice by dividing the period into enough thin layers of given number S [48]. Therefore, m_p can be written as

$$m_p(z_j) = \frac{1}{t_p(z_j)} \begin{bmatrix} [t_p(z_j)^2 - r_p(z_j)^2] & r_p(z_j) \\ -r_p(z_j) & 1 \end{bmatrix}, \tag{7}$$

with $j \in (1, S)$, the elementary reflection coefficient r_p, and transmission coefficient t_p determined by the complex refractive index n_p. Then, the matrix M_p^k of the kth period is

$$M_p^k = m_p(z_1) \times \cdots \times m_p(z_j) \times \cdots \times m_p(z_S). \tag{8}$$

With the transfer matrix M_p^L, we can solve the equation

$$e^{2i\kappa_p a_0} - \mathrm{Tr}\big(M_p^k\big) e^{i\kappa_p a_0} + 1 = 0 \tag{9}$$

to check the dispersion and extinction rate (ω vs κ_p, the Bloch wave vector $\kappa_p = \kappa_p' + i\kappa_p''$) for an infinite medium. As is well known, band gaps appear at the edge of the first Brillouin zone $\kappa_p' = \pi/a_0$ and $\kappa_p'' \neq 0$, where the Bragg condition is fulfilled.

In the following, the total 2×2 transfer matrix for this 1D atomic lattice of the finite length $L = Ka_0$ can be written as

$$M_p^L = M_p^1 M_p^2 \cdots M_p^k \cdots M_p^K, \tag{10}$$

which may be used to deal with the 1D problems, and the 3D problems may be solved by Maxwell wave equations approximated by 3D Gaussian functions [33]. Then, with this 2×2 transfer matrix, it is straightforward to obtain the probe reflectivity, transmissivity and absorption:

$$R_p(L) = \left| \frac{M_p^L(12)}{M_p^L(22)} \right|^2,$$

$$T_p(L) = \left| \frac{1}{M_p^L(22)} \right|^2,$$

$$A_p(L) = 1 - R_p(L) - T_p(L). \tag{11}$$

The spectrum property can be expressed by a sufficiently reduced density of state (DOS) for probe photons, i.e., the reflection appears with the reduction of the DOS [49], which is given by

$$D_p(z) = \mathrm{Re} \left| \frac{2 + r_p^+(z) + r_p^-(z)}{1 - r_p^+(z) r_p^-(z)} - 1 \right| \tag{12}$$

by using the complex reflection coefficients $r_p^+(z)$ and $r_p^-(z)$ of probe fields emitting along the $+z$ axis and $-z$ axis, respectively, and considering a position in the middle of the lattice. It is worth emphasizing that Eq. (12) can be applied for a finite lattice in order to compute the local DOS.

III. RESULTS AND DISCUSSIONS

First, we will check the photonic properties of 1D ordered cold atomic lattices with Gaussian atomic distribution in each period with the randomly called number $\Delta j_{\mathrm{Rand}} = 0$. As shown in Figs. 2(a) and 2(b), there are three frequency regions

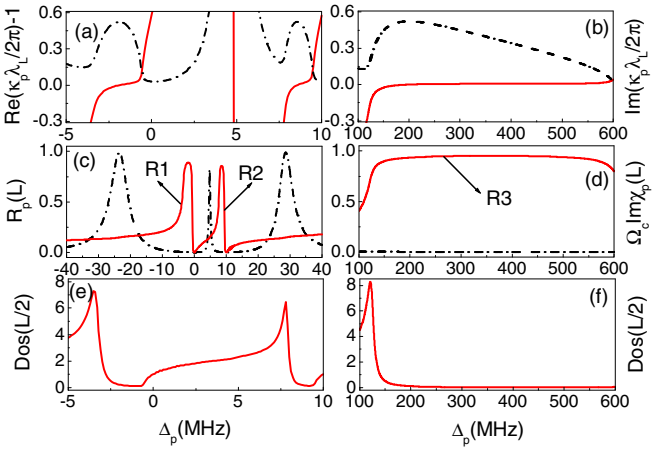

FIG. 2. (a), (b) Real parts (red solid line) and imaginary parts (black dash-dotted line) of Bloch wave vector κ_p. (c), (d) Reflectivities $R_p(L)$ (red solid line) and $\Omega_c\,\mathrm{Im}\,\chi_p(L)$ (black dash-dotted line). (e), (f) DOS of probe field at the center of the lattice as functions of probe detuning Δ_p. Parameters are $\Gamma_{41} = \Gamma_{42} = \Gamma_{43} = \Gamma = 6.0$ MHz, $\Omega_p = 0.048$ MHz, $\Omega_{c1} = \Omega_{c2} = \Omega_c = 3\Gamma$, $\Delta_{c1} = 0.0$ MHz, $\Delta_{c2} = 10.0$ MHz, $\lambda_{\mathrm{Lat}0} = 781$ nm, $\lambda_{p0} = 780.24$ nm, $\Delta\lambda_{\mathrm{Lat}} = 0.5$ nm, $\sigma_z = \lambda_{\mathrm{Lat}}/(4\pi\sqrt{2\eta})$, $\eta = 5$, $L = 3.0$ mm, $N_0 = 7\times10^{11}$ cm^{-3}, $d_{14} = 2.0\times10^{-29}$ C m.

of $\kappa_p'\lambda_{\mathrm{Lat}}/2\pi = 1$ and $\kappa_p'' \neq 0$ corresponding to the forbidden band for light propagation. Figures 2(c) and 2(d) of the probe reflection and transmission spectra further show that three reflection regions of high reflectivity appear in three different frequency regions. The first two narrow reflection regions appear in the EIT windows (near the resonance) at $\Delta_p \subseteq -5 \sim 0$ MHz (denoted by R1) and $7.5 \sim 10$ MHz (denoted by R2), while the third wide one (denoted by R3) locates at the off-resonance region. The physical reason can be expressed as follows. In the field-atom system of periodic structure, the condition of the existence of the perfect reflection is the cooperation between satisfying Bragg scattering and decreasing light absorption. Among the three-color reflections, two narrow ones appear in two EIT windows due to such a tripod-type structure, and the wide one in the far-detuning range without loss due to the far resonance. Figures 2(e) and 2(f) show the local DOSs in and out of the frequency range of reflection regions, which can relatively intuitively describe the existent of photons inside the sample. The reflections arise corresponding to the obvious reduction of local DOSs because of the attenuation solution of the Bloch wave-vector loss, which means there is a propagation solution mismatch between the incident wave and optical latices, related to the evanescent wave.

Though there are three high reflections $R1$, $R2$, and $R3$ ($> 83\%$), we focus on the two narrow EIT reflections ($R1$ for $\Delta_p = \Delta_{c1}$, $R2$ for $\Delta_p = \Delta_{c2}$) due to their dynamic control by adjusting the coupling fields. Moreover, the narrow spectra have good practical applications for the photon modulation in the light-atom interaction.

Figure 3(a) shows the tunability of reflections by one coupling detuning Δ_{c2} in the case of single-photon resonance ($\Delta_{c1} = 0$). As expected, the reflectivities of two reflections $R1$ and $R2$ can reach to 90%; however, $R1$, due to its nearness

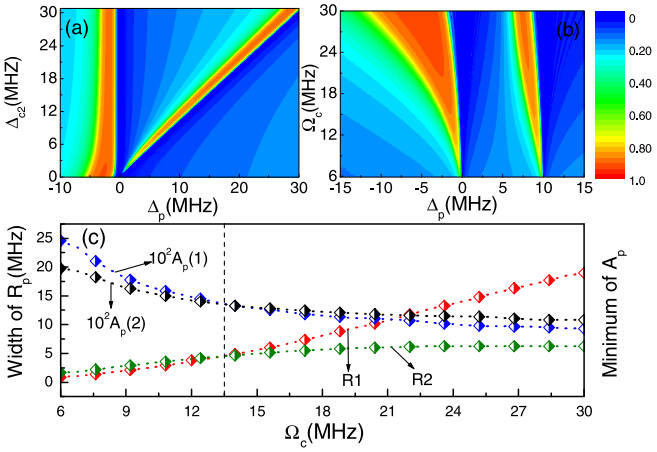

FIG. 3. Plots of EIT reflections $R1$ and $R2$ vs probe detuning Δ_p and coupling detuning Δ_{c2}, with (a) $\Omega_{c1} = \Omega_{c2} = \Omega_c = 3\Gamma$ and (b) Rabi frequency of coupling fields Ω_c. (c) The widths of reflections ($R1$ and $R2$) and the minimum of absorptions [$A_p(1)$ and $A_p(2)$] vs Rabi frequency of coupling fields Ω_c. Other parameters are the same as Fig. 2.

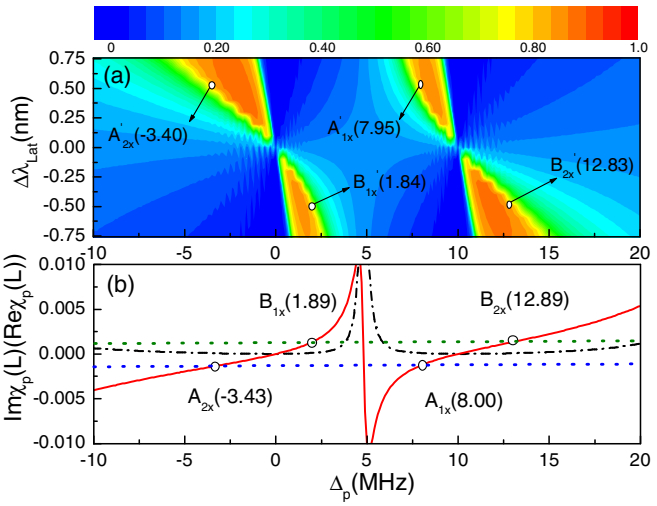

FIG. 4. (a) EIT reflections $R1$ and $R2$ vs probe detuning Δ_p and Bragg detuning $\Delta\lambda_{\rm Lat}$. (b) Real parts (red solid line) and imaginary parts (black dash-dotted line) of average probe susceptibilities vs probe detuning Δ_p, where the two horizonal dots are given by $-2\Delta\lambda_{\rm Lat}/\lambda_{\rm Lat}$ ($\Delta\lambda_{\rm Lat} = 0.5$ nm for blue dots and $\Delta\lambda_{\rm Lat} = -0.5$ nm for olive dots). Other parameters are the same as Fig. 2.

of $\Delta_p = 0$, is obviously wider than $R2$, though the width of $R2$ is increased while that of $R1$ is slightly decreased with increasing Δ_{c2}. Respectively, the two reflections merge into a large wide one following the two-photon resonance ($\Delta_{c1} = \Delta_{c2} = 0$) [see Fig. 3(a)]. Figure 3(b) shows the influence of coupling intensities on the reflections. It is found that the reflectivities and widths of both reflection regions are increased with increasing Ω_c. In particular, $R1$ is much more sensitive to the intensities of the coupling fields, whose reflectivity is greater than 90% with $\Omega_c \geqslant 3\Gamma$ [see Fig. 3(b)]. Essentially, the change in the reflectivity and width of reflection is decided by that of the EIT property. Respectively, the absorption lines become more and more smooth, with the minimum of $A_p(1)$ almost lower than 0.1. There is little difference between the minima of $A_p(1)$ and $A_p(2)$, which results in a straightforward variation of reflections, though the widths of the two reflections are obviously distinct. It is of special interest that double EIT reflections of relatively narrow width and high reflectivity can be obtained by modulating the coupling fields at $\Omega_c \simeq 13.5$ MHz [see Fig. 3(c)].

As mentioned above, the Bragg scattering condition is fundamental for the generation of PBGs; then its influence will be checked by varying the Bragg detuning $\Delta\lambda_{\rm Lat}$ (the lattice wavelength) either in the red detuning $\Delta\lambda_{\rm Lat} > 0$ or in the blue one $\Delta\lambda_{\rm Lat} < 0$. As shown in Fig. 4(a), both reflections become increasingly wider with increasing $|\Delta\lambda_{\rm Lat}|$, but the reflectivities decrease. It is worth noting that when $\Delta\lambda_{\rm Lat} \sim 0$, the probe susceptibility is about zero so that there are inefficient reflections, even though the Bragg condition is fulfilled. That is why a small angle θ is needed for the phase matching. It is interesting that two EIT reflections have a good symmetry relative to the point of $\Delta_p = (\Delta_{c1} + \Delta_{c2})/2$ which intersects $\Delta\lambda_{\rm Lat} = 0$ by modulating $\Delta\lambda_{\rm Lat}$ from negative to positive. It can be explicated clearly by Eq. (6), i.e., the imaginary part of the susceptibility $\chi''_p = 0$ and the real part $\chi'_p \simeq -2\Delta\lambda_{\rm Lat}/\lambda_{\rm Lat}$ for satisfying the Bragg condition, which means the positions of the appearance of the reflections are the points where the horizonal line $(-2\Delta\lambda_{\rm Lat}/\lambda_{\rm Lat})$ intersects with Reχ_p and locate in the EIT windows (Imχ_p is zero). We can clearly see the specific points A_{1x} and A_{2x} (B_{1x} and B_{2x}) [see Fig. 4(b)] corresponding to the points A'_{1x} and A'_{2x} (B'_{1x} and B'_{2x}) [see Fig. 4(a)] with the reflections higher than 80% for $\Delta\lambda_{\rm Lat} = 0.5$ nm ($\Delta\lambda_{\rm Lat} = -0.5$ nm).

Finally, we examine PBGs in a 1D disorder atomic lattice, while considering the atom number fluctuation as a common kind of disorder. Specifically, a lossy atomic lattice has been used with disorder distribution of atomic number density. In this system, we only consider that the atom number fluctuates along z. Because the tightly trapped cold atoms have Gaussian density distribution with a little width $\sigma_z \simeq a_0/7$ in each period, and $a_0 = \lambda_{\rm Lat}/2$, even the small range of the atomic fluctuations is also obvious. However, the transverse range of the motion of atoms depends on the waist of light that forms the optical lattice, which is more than $10\lambda_{\rm Lat}$. So the perturbed disorder along the transverse has a small effect on the atomic density, and thus the transverse fluctuations have been ignored in our regime.

Here we use the random number $\Delta j_{\rm Rand}$ through the lattice as shown in Eq. (1); Fig. 5(a) shows the Gaussian (Gaussian-like) atomic number distribution without (with) the disorder in one period, where the black solid line with triangles describes that without disorder when $\Delta j_{\rm Rand} = 0$ and the red solid line with circles (olive solid line with squares) shows that with a slight (drastic) vertical fluctuation when $\Delta j_{\rm Rand} \in (-0.1, +0.1)$ [$\Delta j_{\rm Rand} \in (1, +1)$]. Then, as displayed in Fig. 5(b), compared with that in the order lattice, the two reflection regions just change a little with considering the atomic number fluctuation, i.e., only $R1$ becomes slightly wider even with the random $\Delta j_{\rm Rand}$ in the maximum random range $(-1, +1)$. Thus, the two EIT reflections show strong robustness that is immune to this disorder. It is worth emphasizing that the scattering mean-free path is much less than

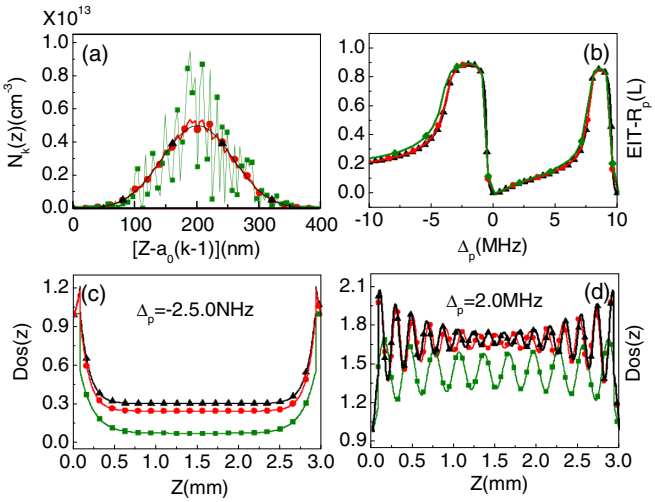

FIG. 5. (a) Atomic density distribution in the kth cell. (b) Reflections $R1$ and $R2$ vs probe detuning Δ_p. (c) DOS of probe photons ω_p at the center of $R1$ for $\Delta_p = -2.5$ MHz. (d) DOS of probe photons ω_p outside $R1$ and $R2$ for $\Delta_p = 2.0$ MHz in the 1D order lattice (black solid line with triangle) and in the disorder lattices for $\Delta j_{\text{Rand}} \in (-0.1, +0.1)$ (red solid line with circle) and $\Delta j_{\text{Rand}} \in (-1.0, +1.0)$ (olive solid line with square). Other parameters are the same as Fig. 2.

the size of the system with the small number fluctuation such as $\Delta j_{\text{Rand}} \in (-0.1, +0.1)$. As a result, the system may be in the localized regime. When it is relatively long, corresponding to the large number fluctuation, even reaching the maximum $\Delta j_{\text{Rand}} \in (-1.0, +1.0)$, the scattering mean-free path is almost the size of the sample. Then, the system may be regarded as the ballistic one.

Furthermore, the robustness can also be observed via the DOSs. In the order and disorder optical lattices, Figs. 5(c) and 5(d) show the DOSs of $\Delta_p = -2.5$ MHz in the frequency range of the reflection $R1$ and ones of $\Delta_p = 2.0$ MHz out of the frequency range of two reflection regions as functions of the lattice axis z, respectively. It is clear that compared with those in the order lattice, the DOSs may all decrease with the increasing of the random fluctuation range, which means the existence of a photon in the sample may be suppressed to a certain extent due to the atomic fluctuation. In particular, in Fig. 5(c), the DOSs in the range of the reflection regions always remain very low in the lattice, which implies the photons also are prevented from propagating through the lattice by the robust photonic gaps of high reflectivity. However, the DOSs out of the range of the reflection regions not only decrease but also oscillate more obviously, especially in the middle of the sample. The behavior of photons inside the sample may be more sensitive to the atomic fluctuation. In general, as expected, such a tunable reflection scheme has strong robustness for forbidding propagation in the photonic gaps.

IV. CONCLUSIONS

To summarize, we presented a study of multicolor reflections in a sample of cold atoms driven into a four-level tripod-type EIT configuration trapped in a 1D order and disorder optical lattice. In our system, there are three reflection regions of high reflectivity, and two narrow ones near a two-photon resonance located in two EIT windows and another one in the large detuning range. The narrow and high EIT reflection regions attract our attention because of their excellent tunability in terms of relevant parameters of the coupling fields and atomic lattice. In particular, under the Bragg scattering condition, the position and width of the reflections can be modulated via controlling the frequency and intensity of the coupling fields, the Bragg detuning. In addition, we examine the effect of a typical kind of disorder in the atomic lattice, i.e., atomic number fluctuation, on the photonic band gaps. It is noted that this reflection scheme is immune to the disorder, and photonic properties in the frequency range of such photonic gaps exhibit strong robustness. Here, all ordered ^{87}Rb atoms are chosen with Zeeman sublevels via the circularly polarized optical pumping technique, in regard to a possible experiment. Therefore, such a robust reflection scheme may be used to explore all-optical switching and routing devices involving multicolor photons.

ACKNOWLEDGMENTS

This work is supported by the Natural Science Foundation of Hainan Province(Grant No. 118QN230), the National Natural Science Foundation of China (Grants No. 11861031 and No. 11704064), Key Laboratory of Laser Technology and Optoelectronic Functional Materials of Hainan Province, Jilin Scientific and Technological Development Program (Grant No. 20180520205JH), and the Fundamental Research Funds for the Central Universities (Grant No. 2412019FZ045).

[1] G.-W. Lin, S.-C. Zhang, Y.-Q. Hu, Y.-P. Niu, J.-B. Gong, and S.-Q. Gong, Phys. Rev. Lett. **123**, 033902 (2019).
[2] S.-C. Zhang, Y.-Q. Hu, G.-W. Lin, Y.-P. Niu, K.-Y. Xia, J.-B. Gong, and S.-Q. Gong, Nat. Photon. **12**, 744 (2018).
[3] M. Litinskaya and E.-A. Shapiro, Phys. Rev. A **91**, 033802 (2015).
[4] L. Xu, H.-X. Wang, Y.-D. Xu, H.-Y. Chen, and J.-H. Jiang, Opt. Express **24**, 18059 (2016).
[5] C. Q. Cook and A. Amir, Optica **3**, 1436 (2016).
[6] A. Cerjan and S. Fan, Phys. Rev. A **96**, 051802(R) (2017).
[7] M. Klimczak, D. Michalik, G. Stepniewski, T. Karpate, J. Cimek, X. Forestier, R. kasztelanic, D. Pysz, R. Stepien, and R. Buczynski, J. Opt. Soc. Am. B **36**, A112 (2019).
[8] A. Frolich, J. Fischer, C. Wolff, K. Busch, and M. Wegener, Adv. Opt. Mater. **2**, 849 (2014).
[9] I. Staude, M. Thiel, S. Essig, C. Wolff, K. Busch, G.-V. Freymann, and M. Wegener, Opt. Lett. **35**, 1094 (2010).
[10] L.-F Chen, M.-P.-C. Taverne, X. Zheng, J.-D. Lin, R. Oulton, M. Lopez-Garcia, Y.-L.-D. Ho, and J.-G. Rarity, Opt. Express **23**, 26565 (2015).

[11] H.-W. Dong, Y.-S. Wang, T.-X. Ma, and X.-X. Su, J. Opt. Soc. Am. B **31**, 2946 (2014).
[12] A.-H. Safavi-Naeini, J.-T. Hill, S. Meenehan, J. Chan, S. Groblacher, and O. Painter, Phys. Rev. Lett. **112**, 153603 (2014).
[13] N. Chamanara, S. Taravati, Z.-L. Deck-Leger, and C. Caloz, Phys. Rev. B **96**, 155409 (2017).
[14] S.-A. Hack, J. J.-W. van der Vegt, and W. L. Vos, Phys. Rev. B **99**, 115308 (2019).
[15] T. Yoon and M. Bajcsy, Phys. Rev. A **99**, 023415 (2019).
[16] D. Devashish, O. S. Ojambati, S. B. Hasan, J. J. W. van der Vegt, and W. L. Vos, Phys. Rev. B **99**, 075112 (2019).
[17] T. Sunner, T. Stichel, S.-H. Kwon, T.-W. Schlereth, S. Hofling, M. Kamp, and A. Forchel, Appl. Phys. Lett. **92**, 261112 (2008).
[18] K. Nozaki, T. Tanabe, A. Shinya, S. Matsuo, T. Sato, H. Taniyama, and M. Notomi, Nat. Photon. **4**, 477 (2010).
[19] S. John, Nat. Mater. **11**, 997 (2012).
[20] M. Khajavikhan, A. Simic, M. Katz, J.-H. Lee, B. Slutsky, A. Mizrahi, V. Lomakin, and Y. Fainman, Nature (London) **482**, 204 (2012).
[21] L. Yang, Y. Zhang, X.-B. Yan, Y. Sheng, C.-L. Cui, and J.-H. Wu, Phys. Rev. A **92**, 053859 (2015).
[22] Y. Zhang, Y.-M. Liu, T.-Y. Zheng, and J.-H. Wu, Rev. A **94**, 013836 (2016).
[23] J.-H. Wu, M. Artoni, and G. C. La Rocca, Phys. Rev. A **91**, 033811 (2015).
[24] J.-H. Wu, M. Artoni, and G. C. La Rocca, Phys. Rev. A **95**, 053862 (2017).
[25] Y.-M. Liu, F. Gao, C.-H. Fan, and J.-H. Wu, Opt. Lett. **42**, 4283 (2017).
[26] G. Birkl, M. Gatzke, I. H. Deutsch, S. L. Rolston, and W. D. Phillips, Phys. Rev. Lett. **75**, 2823 (1995).
[27] D. Petrosyan, Phys. Rev. A **76**, 053823 (2007).
[28] A. Schilke, C. Zimmermann, P. W. Courteille, and W. Guerin, Phys. Rev. Lett. **106**, 223903 (2011).
[29] A. Schilke, C. Zimmermann, and W. Guerin, Phys. Rev. A. **86**, 023809 (2012).
[30] H. Yang, L. Yang, X.-C. Wang, C.-L. Cui, Y. Zhang, and J.-H. Wu, Phys. Rev. A **88**, 063832 (2013).
[31] X.-M. Su and B.-S. Ham, Phys. Rev. A. **71**, 013821 (2005).
[32] M. Artoni and G. C. La Rocca, Phys. Rev. Lett. **96**, 073905 (2006).
[33] J.-H. Wu, M. Artoni, and G. C. La Rocca, J. Opt. Soc. Am. B. **25**, 1840 (2008).
[34] J.-W. Gao, Y. Zhang, N. Ba, C.-L. Cui, and J.-H. Wu, Opt. Lett. **35**, 709 (2010).
[35] Y. Zhang, J.-W. Gao, C.-L. Cui, Y. Jiang, and J.-H. Wu, Phys. Lett. A **374**, 1088 (2010).
[36] Y. Zhang, Y. Xue, G. Wang, C.-L. Cui, R. Wang, and J.-H. Wu, Opt. Express **19**, 2111 (2011).
[37] C. Hang, G. Huang, and V. V. Konotop, Phys. Rev. Lett. **110**, 083604 (2013).
[38] V. G. Arkhipkin and S.-A. Myslivets, Phys. Rev. A **93**, 013810 (2016).
[39] N. V. Corzo, B. Gouraud, A. Chandra, A. Goban, A.-S. Sheremet, D.-V. Kupriyanov, and J. Laurat, Phys. Rev. Lett. **117**, 133603 (2016).
[40] J. Gao, L.-F. Qiao, X.-F. Lin, Z.-Q. Jiao, Z. Feng, Z. Zhou, Z.-W. Gao, X.-Y. Xu, Y. Chen, H. Tang, and X.-M. Jin, Opt. Express **24**, 12607 (2016).
[41] A. Rakonjac, A. L. Marchant, T. P. Billam, J. L. Helm, M. M. H. Yu, S. A. Gardiner, and S. L. Cornish, Phys. Rev. A **93**, 013607 (2016).
[42] J.-P. Covey, S. A. Moses, M. Garttner, A. S. Naini, M. T. Miecnikowski, Z. K. Fu, J. Schachenmayer, P. S. Julienne, A. M. Rey, D. S. Jin, J. Ye, Nat. Commun. **7**, 11279 (2016).
[43] M. Yan, H. Y. Hui, M. Rigo, and V. W. Scarola, Phys. Rev. Lett. **119**, 073002 (2017).
[44] C. Meldgin, Ph.D. thesis, The University of Illinois at Urbana-Champaign, 2016.
[45] J.-H. Wu, M. Artoni, and G. C. La Rocca, Phys. Rev. Lett. **103**, 133601 (2009).
[46] Z. W. Barber, C. W. Hoyt, C. W. Oates, L. Hollberg, A. V. Taichenachev, and V. I Yudin, Phys. Rev. Lett. **96**, 083002 (2006).
[47] M.-J. Lu and J. D. Weinstein, Opt. Lett. **35**, 622 (2010).
[48] M. Artoni, G. La Rocca, and F. Bassani, Phys. Rev. E **72**, 046604 (2005).
[49] G. Boedecker and C. Henkel, Opt. Express **11**, 1590 (2003).